A hybrid FEM for solving the Allen–Cahn equation

Jaemin Shin [a], Seong-Kwan Park [b], Junseok Kim [c],*

[a] Institute of Mathematical Sciences, Ewha W. University, Seoul 120-750, Republic of Korea
[b] Department of Mathematics, Yonsei University, Seoul 120-749, Republic of Korea
[c] Department of Mathematics, Korea University, Seoul 136-713, Republic of Korea

ARTICLE INFO

ABSTRACT

We present an unconditionally stable hybrid finite element method for solving the Allen–Cahn equation, which describes the temporal evolution of a non-conserved phase-field during the antiphase domain coarsening in a binary mixture. Its various modified forms have been applied to image analysis, motion by mean curvature, crystal growth, topology optimization, and two-phase fluid flows. The hybrid method is based on the operator splitting method. The equation is split into a heat equation and a nonlinear equation. An implicit finite element method is applied to solve the diffusion equation and then the nonlinear equation is solved analytically. Various numerical experiments are presented to confirm the accuracy and efficiency of the method. Our simulation results are consistent with previous theoretical and numerical results.

© 2014 Elsevier Inc. All rights reserved.

1. Introduction

To model antiphase domain coarsening in a binary alloy, the following Allen–Cahn (AC) equation was introduced [1]:

$$\frac{\partial \phi(\mathbf{x}, t)}{\partial t} = -\frac{F'(\phi(\mathbf{x}, t))}{\epsilon^2} + \Delta \phi(\mathbf{x}, t), \quad \mathbf{x} \in \Omega, \ t > 0, \tag{1}$$

where $\Omega \subset \mathbb{R}^2$ is a domain. The quantity $\phi(\mathbf{x}, t)$ is defined as the difference of concentrations $\phi = c_A - c_B$, where c_A and c_B are the mass fractions of components A and B in a binary mixture. The function $F(\phi) = 0.25(\phi^2 - 1)^2$ is the Helmholtz free energy density. The small positive constant ϵ is the gradient energy coefficient related to the interfacial energy. The system is completed by taking initial and natural boundary conditions $\mathbf{n} \cdot \nabla \phi = 0$, where $\mathbf{n}$ is normal to $\partial \Omega$. The AC equation is a gradient flow with the Ginzburg–Landau free energy

$$\mathcal{E}(\phi) := \int_\Omega \left(\frac{F(\phi)}{\epsilon^2} + \frac{|\nabla \phi|^2}{2} \right) d\mathbf{x}.$$

To show the total energy $\mathcal{E}(\phi)$ is non-increasing in time, we differentiate the energy $\mathcal{E}(\phi)$ with respect to time t

$$\frac{d\mathcal{E}(\phi)}{dt} = \int_\Omega \left(\frac{F'(\phi)}{\epsilon^2} \phi_t + \nabla \phi \cdot \nabla \phi_t \right) d\mathbf{x} = \int_\Omega \left(\frac{F'(\phi)}{\epsilon^2} - \Delta \phi \right) \phi_t d\mathbf{x} + \int_{\partial \Omega} (\mathbf{n} \cdot \nabla \phi) \phi_t ds = -\int_\Omega \phi_t^2 d\mathbf{x} \leqslant 0,$$

where we have used the homogeneous Neumann boundary condition. The AC equation has been solved by using various numerical approaches such as the finite element, finite difference, and Fourier-spectral methods [2–7]. The various modified forms of AC equation have been applied to image analysis [8–10], motion by mean curvature [11–14], crystal growth [15,16], topology optimization [17,18], and two-phase fluid flows [19,20]. In general, finite element method (FEM) is better than finite difference method (FDM) in dealing with complicated domain problems. In FDM framework, a hybrid scheme was used in [3]. However, it is not used in FEM. Therefore, the objective of this paper is to develop an unconditionally stable hybrid finite element method for solving the Allen–Cahn equation.

This paper is organized as follows. In Section 2, we describe the numerical solution algorithm of the AC equation. The numerical results showing the robustness and superiority of the proposed scheme are presented in Section 3. In Section 4, conclusions are drawn.

2. Numerical solution

We present an unconditionally stable hybrid scheme for solving the AC equation using the finite element method. Let $H^1(\Omega)$ denote the trial solution space. We partition Ω into a set $\mathcal{T}_h$ consisting of a triangular element τ. Let $V_h = \{\psi \in C(\bar{\Omega}) : \psi|_\tau \text{ is linear } \forall \tau \in \mathcal{T}_h\} \subset H^1(\Omega)$ be the finite element space. Let $\{x_i\}_{i=1}^N$ be the nodes of $\mathcal{T}_h$ and let $\{\eta_i\}_{i=1}^N$ be the linear basis functions such that $\eta_i \in V_h, \eta_i(x_j) = \delta_{ij}$, for $i,j = 1, \cdots, N$, where N is the dimension of the discrete space. We denote ϕ_i as the approximation of $\phi(x_i)$ and define as $\phi_h = \sum_{i=1}^N \phi_i \eta_i$. We formally split the AC equation (1) into the heat and nonlinear differential equations as follows:

$$\frac{\partial \phi(\mathbf{x},t)}{\partial t} = \Delta \phi(\mathbf{x},t), \tag{2}$$

$$\frac{\partial \phi(\mathbf{x},t)}{\partial t} = -\frac{F'(\phi(\mathbf{x},t))}{\epsilon^2}. \tag{3}$$

We numerically solve Eq. (2) by using a fully implicit finite element method and analytically solve Eq. (3) by using the method of separation of variables. First, given ϕ_h^n, the finite element approximation to Eq. (2) is to find ϕ_h^* such that for all $\psi_h \in V_h$

$$\left(\frac{\phi_h^* - \phi_h^n}{\Delta t}, \psi_h\right) + (\nabla \phi_h^*, \nabla \psi_h) = 0, \tag{4}$$

where Δt is the time step and $(\cdot, \cdot)$ is the inner product. Eq. (4) leads to the standard Galerkin method $(M + \delta t K)\phi_h^* = M\phi_h^n$, where $M = (m_{ij})$ and $K = (k_{ij})$ are the mass and stiffness matrices with elements $m_{ij} = (\eta_i, \eta_j)$ and $k_{ij} = (\nabla \eta_i, \nabla \eta_j)$. Because the standard Galerkin method does not guarantee the maximal principle [22], we use the lumped mass method $(\bar{M} + \delta t K)\phi_h^* = \bar{M}\phi_h^n$, where $\bar{M}$ obtained by taking for its diagonal elements $\bar{m}_{ii} = \sum_{j=1}^N m_{ij}$. For the implementation, we refer to [21]. Second, by the method of separation of variables, Eq. (3) is solved analytically with the initial condition ϕ_h^*.

$$\phi_h^{n+1} = \frac{\phi_h^*}{\sqrt{\epsilon^{-\frac{2\Delta t}{\epsilon^2}} + (\phi_h^*)^2 \left(1 - e^{-\frac{2\Delta t}{\epsilon^2}}\right)}}. \tag{5}$$

In summary, to calculate ϕ_h^{n+1} from ϕ_h^n, we solve Eqs. (4) and (5).

The stability of the proposed numerical scheme should be studied to get a reasonable solution. We prove that the proposed scheme is unconditionally stable. Assume that $\|\phi^n\|_\infty \leqslant 1$. The stability analysis [22] shows that the lumped mass method of Eq. (4) is unconditionally stable. In addition, the inequality $|\phi^*| \leqslant \|\phi^n\|_\infty$ is satisfied by the maximal principle for the heat equation, and it implies that $\|\phi^*\|_\infty \leqslant 1$. And, for the Eq. (5), we have the inequality

$$|\phi_i^{n+1}| = \frac{|\phi_i^*|}{\sqrt{e^{-\frac{2\Delta t}{\epsilon^2}} + (\phi_i^*)^2 \left(1 - e^{-\frac{2\Delta t}{\epsilon^2}}\right)}} = \frac{1}{\sqrt{1 + \left(\frac{1}{(\phi_i^*)^2} - 1\right)e^{-\frac{2\Delta t}{\epsilon^2}}}} \leqslant 1 \tag{6}$$

Therefore, we can conclude that if $\|\phi^n\|_\infty \leq 1$, then $\|\phi^{n+1}\|_\infty \leq 1$. And, because the initial condition is given as $\|\phi^0\|_\infty \leq 1$, the proposed scheme is stable for any time step size.

3. Numerical results

We perform numerical tests such as a convergence test, phase separation, and motion by mean curvature to validate the accuracy and efficiency of the proposed method.

3.1. The convergence test

We demonstrate that the numerical scheme is first- and second-order accurate in time and space, respectively. A quantitative estimate of convergence rate is obtained by performing a number of simulations with a set of decreasing space or time step size. For the test problem, we use the traveling wave solution of Eq. (1)

$$\phi(x, y, t) = \frac{1}{2}\left(1 - \tanh\frac{x - st}{2\sqrt{2}\epsilon}\right),$$

where $s = 3/\left(\sqrt{2}\epsilon\right)$ is the speed of the traveling wave [2]. The numerical solution with the initial condition $\phi(x, y, 0)$ is solved on the computational domain $\Omega = (-1, 1) \times (-1, 1)$. The mesh is the set of regular triangular elements as shown in Fig. 1. We denote the mesh step size h as the length of legs of right triangles on the regular mesh.

The error of the numerical solution is defined as $e = (e_1, e_2, \ldots, e_N)$, where $e_i = \phi_i^{N_t} - \phi_i(T)$ for $i = 1, \ldots, N$. For each test, we evolve the discrete equations to time $T = 0.25/s$ with $\epsilon = 0.03$ and $h = 2^{-7}$. To estimate the rate of convergence for time, $\Delta t = 0.01/2^{n-1}$ are used for $n = 1, 2, 3, 4$. To estimate the rate of convergence for space, the parameters $\Delta t = T/10^4$ and $h = 2^{-n}$ are used for $n = 3, 4, 5, 6$. Tables 1 and 2 show the discrete l_2 and maximum norms of the errors and rates of convergence for time and space, respectively. These results show that the scheme is indeed first- and second-order accurate in time and space, respectively.

3.2. Phase separation

We consider the spinodal decomposition of a binary mixture. On the square and circle domains, Fig. 2 shows the evolutions of the phase separation with the initial condition $\phi(x, y, 0) = 0.01 \text{rand}(x, y)$, where $\text{rand}(x, y)$ is a random value between -1 and 1. The time step size $\Delta t = 2E-6$ and $\epsilon = 0.02$ are used. For simulating on the square domain, the domain is $\Omega = (-1, 1) \times (-1, 1)$ with 257×257 mesh grid points. For simulating on the disk, the domain is a disk of which the radius is 1.

Fig. 2 shows the non-increasing trends of the scaled discrete total energy $\mathcal{E}(\phi^n)/\mathcal{E}(\phi^0)$. The dashed and solid lines are the temporal evolutions of the total energies on the rectangular and circular domains, respectively. The inscribed small figures are evolutions at the associated times. We draw the level contours from -0.8 to 0.8 increasing by factor to 0.2. These numerical results agree well with the total energy dissipation property. At the early stage of the phase separation, the diffuse interfaces are smeared and the level contours are widely distributed. On the boundary, the contact angle of the phase is apparently remained to the right angle.

3.3. Mean curvature flow

We present the numerical simulation of surface evolution according to the mean curvature. Eq. (1) was formally shown that the zero level contour of ϕ evolves to the normal direction velocity V with the mean curvature κ [1,23]. In two dimensional space,

$$V = -\kappa = -1/R, \tag{7}$$
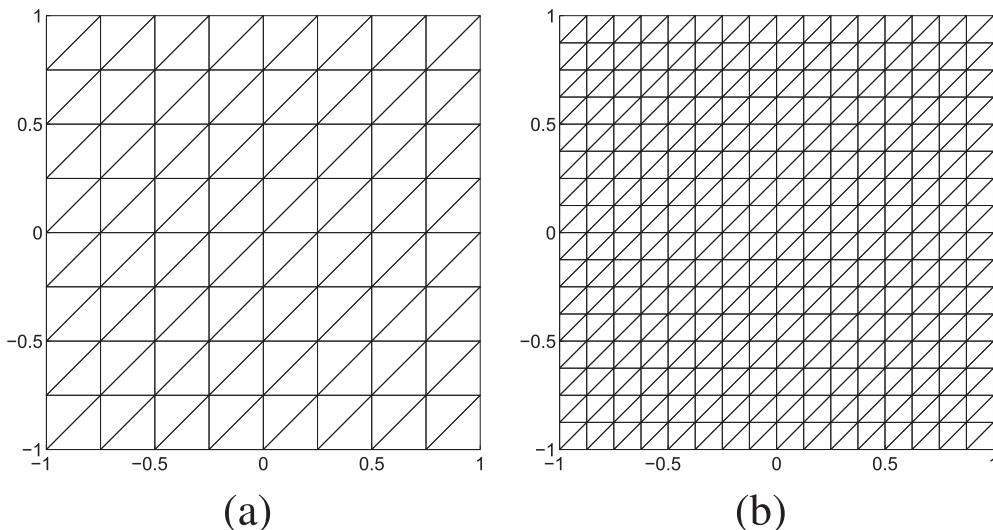
Fig. 1. Regular triangular mesh: (a) 9×9 and (b) 17×17 mesh grids.

Table 1
The errors and rates of convergence for time.

Δt	$0.05/s$	Rate	$0.025/s$	Rate	$0.0125/s$	Rate	$0.00625/s$
$\|e\|_\infty$	3.48E−3	0.99	1.75E−3	0.99	8.82E−4	0.92	4.66E−4

Table 2
The errors and rates of convergence for space.

Mesh	17×17	Rate	33×33	Rate	65×65	Rate	129×129
$\|e\|_\infty$	5.05E−2	1.61	1.66E−2	2.38	3.17E−3	2.24	6.72E−4
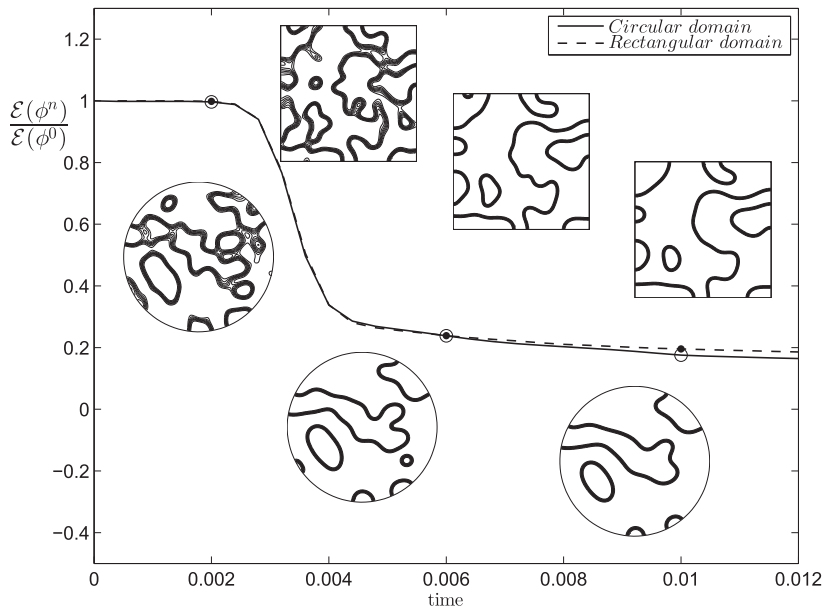
Fig. 2. Non-dimensional discrete total energy $\mathcal{E}(\phi^n)/\mathcal{E}(\phi^0)$.

where R is the radius of curvature at the point on the curve. If we set the initial condition as the circular region and denote the initial radius as R_0. The radius at time t is denoted as $R(t)$. Then Eq. (7) becomes $dR(t)/dt = -1/R(t)$. The solution is $R(t) = \sqrt{R_0^2 - 2t}$. Thus the area $A(t)$ at time t is $A(t) = \pi\left(R_0^2 - 2t\right)$.

Fig. 3(a) shows the temporal evolution of two-dimensional circular shape. The initial condition is given by a circle where the center is $(0,0)$ with a radius 0.9, which is the ticker line. Fig. 3(b) shows the decreasing area due to the motion by mean curvature. The solid line is an exact area and the circles are the numerical area. For the initial condition, we set as $\phi(x,y,0) = \tanh[(0.9 - \sqrt{x^2 + y^2})/(\sqrt{2}\epsilon)]$ on the computational domain $\Omega = (-1,1) \times (-1,1)$ with 257×257 grid points, time step size $\Delta t = 1E{-}6$, and $\epsilon = 0.0188$.

Fig. 4 shows the evolution of a star-shaped interface in a curvature-driven flow on the computational domain $\Omega = (-2,2) \times (-1,1)$. The regular mesh contains 257×129 grid points. The other parameters are $\Delta t = 1E{-}5$ and $\epsilon = 0.0075$. The initial configuration is defined as follows: $\phi(x,y,0) = \tanh\left(d(x,y)/(\sqrt{2}\epsilon)\right)$, where

$$d(x,y) = 0.6 + 0.2\sin(5\theta) - \sqrt{0.25x^2 + y^2} \tag{8}$$

and $\theta = \text{atan2}(y,x)$, which is a variation of the arc-tangent function in computer languages. The tips of the star move inward, while the gaps between the tips move outward. Once the form deforms to a circular shape, the radius of the circle shrinks with increasing speed.

Fig. 5 shows the temporal evolution of the rectangular shape. The initial configuration is given by $\phi(x,y,0) = \tanh\left(d(x,y)/(\sqrt{2}\epsilon)\right)$, where

$$d(x,y) = -\max\{|x - 1| - 0.7, |y - 0.5| - 0.1\}. \tag{9}$$

The computation is performed on 257×129 mesh points with $\epsilon = 0.03$ and $\Delta t = 1E{-}5$. The ticker line represents the initial configuration and the succeeding contour lines are incremented by the time interval $5E{-}3$. The tip where the two sides meet

(a) Contours　　　　　(b) Area
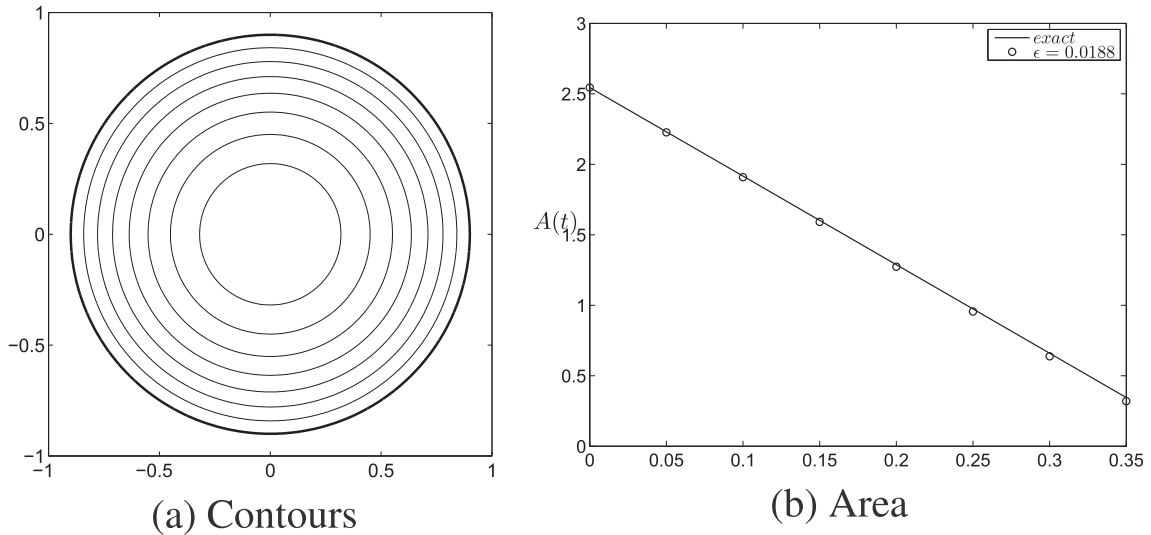
Fig. 3. Mean curvature flow of the circle.
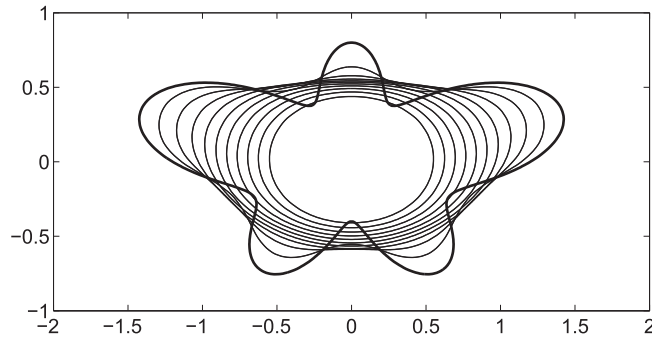
Fig. 4. Evolution of a star-shaped interface in a curvature-driven flow.
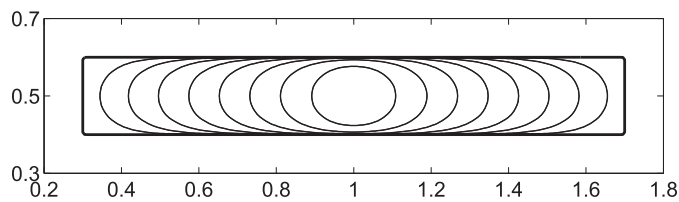
Fig. 5. Temporal evolution of the two-dimensional dumbbell shape.

has a large curvature. The contour lines are shrinking to the center of the rectangle. But lines on the top and bottom side are not evolved until the adjacent sides are curved.

3.4. Complicated domains

Fig. 6 shows the spinodal decomposition on the strip-like domain at $t = 0.02$. Let $C(s) = (0.1s\cos(s), 0.1s\sin(s))$, $\pi < s < 12\pi$, be a smooth curve with its length 11π, where s is the arc length parameter. We define a strip-like domain Ω along $C(s)$ with its width 0.4 by $\Omega = \{C(s) + zv(s) : \pi < s < 12\pi, -0.2 < z < 0.2\}$, where $v(s)$ is a unit normal vector of $C(s)$. The temporal step size $\Delta t = 5\mathrm{E}{-}6$ and $\epsilon = 0.05$ are used. The mesh contains $44,926$ triangular elements and $24,905$ nodes. The initial state is $\phi(x, y, 0) = 0.1\mathrm{rand}(x, y)$. Fig. 6(b) shows the triangular mesh of a part of Fig. 6(a).

Fig. 7 shows the spinodal decomposition on the sequential T-junctions at time $t = 0.0004$. The time step size $\Delta t = 1\mathrm{E}{-}7$ and $\epsilon = 0.005$ are used. The initial state is $\phi^0 = 0.01\mathrm{rand}(x, y)$. The mesh contains $256,611$ triangular elements and $133,720$

(a) Spinodal decomposition   (b) Triangular mesh
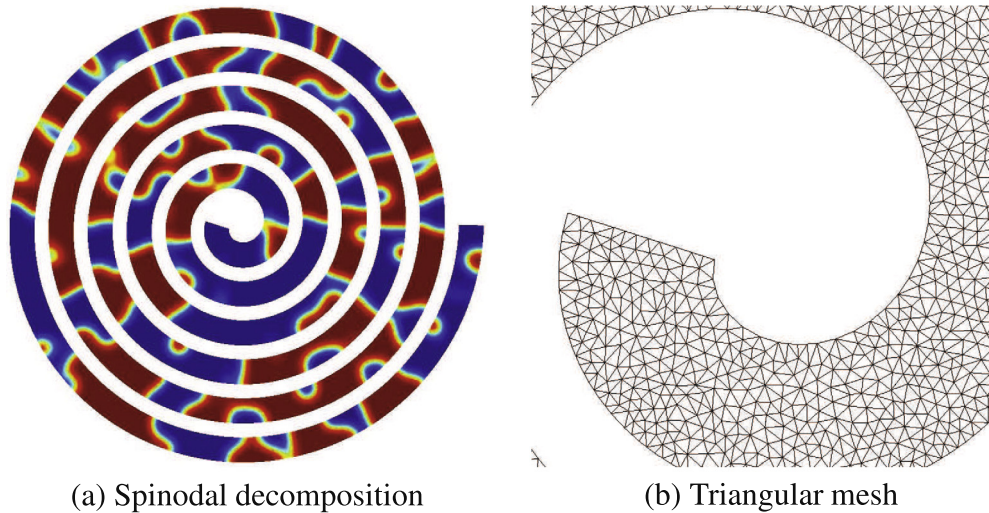
Fig. 6. Snapshot of a later stage of spinodal decomposition in a spiral domain.
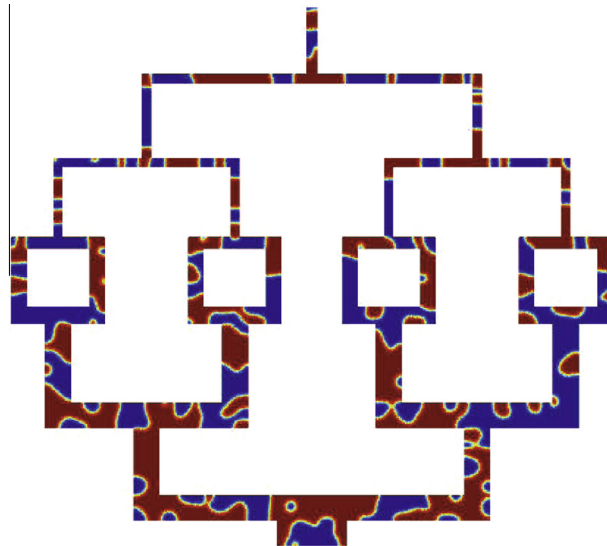
Fig. 7. Snapshot of a later stage of spinodal decomposition in a T-junction domain.

nodes. T-junctions is a micro-fluidic device that offers capabilities for the precise handling of small fluid volumes dispersed as droplets [24].

4. Conclusions

We apply the hybrid numerical scheme for solving AC equation based on the finite element method. We numerically demonstrate the phase separation and non-increasing total energy. And we apply our solver to the examples for simulating the motion by mean curvature and phase separation on the complicated domains.

Acknowledgments

References

[1] S.M. Allen, J.W. Cahn, A microscopic theory for antiphase boundary motion and its application to antiphase domain coarsening, Acta Metall. 27 (1979) 1085–1095.
[2] J.-W. Choi, H.G. Lee, D. Jeong, J. Kim, An unconditionally gradient stable numerical method for solving the Allen–Cahn equation, Physica A 388 (2009) 1791–1803.
[3] Y. Li, H.G. Lee, D. Jeong, J.S. Kim, An unconditionally stable hybrid numerical method for solving the Allen–Cahn equation, Comput. Math. Appl. 60 (2010) 1591–1606.
[4] X. Feng, H. Wu, A posteriori error estimates and an adaptive finite element method for the Allen–Cahn equation and the mean curvature flow, J. Sci. Comput. 24 (2005) 121–146.
[5] R. Kornhuber, R. Krause, Robust multigrid methods for vector-valued Allen–Cahn equations with logarithmic free energy, Comput. Vis. Sci. 9 (2006) 103–116.
[6] A.Q.M. Khaliq, J. Martín-Vaquero, B.A. Wade, M. Yousuf, Smoothing schemes for reaction–diffusion systems with nonsmooth data, J. Comput. Appl. Math. 223 (2009) 374–386.
[7] J. Shen, X. Yang, Numerical approximations of Allen–Cahn and Cahn–Hilliard equations, Discrete Contin. Dyn. Syst. Ser. A 28 (2010) 1669–1691.
[8] M. Beneš, V. Chalupecky, K. Mikula, Geometrical image segmentation by the Allen–Cahn equation, Appl. Numer. Math. 51 (2004) 187–205.
[9] J.A. Dobrosotskaya, A.L. Bertozzi, A Wavelet-Laplace variational technique for image deconvolution and inpainting, IEEE Trans. Image Process. 17 (2008) 657–663.
[10] Z. Rong, L.L. Wang, X.C. Tai, Adaptive wavelet collocation methods for image segmentation using TV–Allen–Cahn type models, Adv. Comput. Math. 38 (2013) 101–131.
[11] M. Beneš, K. Mikula, Simulation of anisotropic motion by mean curvature-comparison of phase field and sharp interface approaches, Acta Math. Univ. Comenian. 67 (1998) 17–42.
[12] L.C. Evans, H.M. Soner, P.E. Souganidis, Phase transitions and generalized motion by mean curvature, Commun. Pure Appl. Math. 45 (1992) 1097–1123.
[13] X. Feng, A. Prohl, Numerical analysis of the Allen–Cahn equation and approximation for mean curvature flows, Numer. Math. 94 (2003) 33–65.
[14] T. Ohtsuka, Motion of interfaces by an Allen–Cahn type equation with multiple-well potentials, Asymptot. Anal. 56 (2008) 87–123.
[15] M. Cheng, J.A. Warren, An efficient algorithm for solving the phase field crystal model, J. Comput. Phys. 227 (2008) 6241–6248.
[16] A.A. Wheeler, W.J. Boettinger, G.B. McFadden, Phase-field model for isothermal phase transitions in binary alloys, Phys. Rev. A 45 (1992) 7424–7439.
[17] L. Blank, M. Butz, H. Garcke, L. Sarbu, V. Styles, Allen–Cahn and Cahn–Hilliard variational inequalities solved with optimization techniques, in: G. Leugering, S. Engell, M. Hinze, R. Rannacher, V. Schulz, M. Ulbrich, S. Ulbrich (Eds.), Constrained Optimization and Optimal Control for Partial Differential Equations, ISNM, vol. 160, pp. 21–35, 2012.
[18] J.S. Choi, T. Yamada, K. Izui, S. Nishiwaki, J. Yoo, Topology optimization using a reaction–diffusion equation, Comput. Methods Appl. Mech. Eng. 200 (2011) 2407–2420.
[19] X. Yang, J.J. Feng, C. Liu, J. Shen, Numerical simulations of jet pinching-off and drop formation using an energetic variational phase-field method, J. Comput. Phys. 218 (2006) 417–428.
[20] J.H. Adler, J. Brannick, C. Liu, T. Manteuffel, L. Zikatanov, First-order system least squares and the energetic variational approach for two-phase flow, J. Comput. Phys. 230 (2011) 6647–6663.
[21] J. Alberty, C. Carstensen, S.A. Funken, Remarks around 50 lines of Matlab: short finite element implementation, Numer. Algorithms 20 (1999) 117–137.
[22] V. Thomee, Galerkin Finite Element Methods for Parabolic Problems, Springer-Verlag, Berlin, 1984.
[23] P.C. Fife, Dynamics of Internal Layers and Diffusive Interfaces, SIAM, Philadelphia, PA, 1988.
[24] D.R. Link, S.L. Anna, D.A. Weitz, H.A. Stone, Geometrically mediated breakup of drops in microfluidic devices, Phys. Rev. Lett. 92 (2004) 054503.